

A Wideband Triple-Mode Differentially-Fed Microstrip Patch Antenna

Xuekang Liu, Wei Hu, Steven Gao, *Fellow, IEEE*, Lehu Wen, Qi Luo, *Senior Member, IEEE*, Peng Fei, Rui Xu, and Ying Liu, *Senior Member, IEEE*

Abstract—A wideband differentially-fed microstrip patch antenna (MPA) with tripe-resonant modes is presented in this letter. The proposed triple-mode MPA is realized by combining two dual-mode MPAs (MPA-I and MPA-II) with different resonant frequency ratios. Firstly, the $TM_{0,1}$ mode and $TM_{0,1/2}$ mode of dual-mode MPA-I can be concurrently excited by adding a pair of coupling shorted patches beside the strip MPA. The ratio of $f_{0,1/2}/f_{0,1}$ can be easily adjusted by moving the shorting pins between the strip MPA and shorted patches. Secondly, by properly designing the dimensions of a conventional MPA, the $TM_{0,1}$ and $TM_{2,1}$ modes of dual-mode MPA-II are simultaneously excited. To further reduce the ratio of $f_{2,1}/f_{0,1}$, four slots are elaborately etched on the conventional MPA. Finally, by combining the two dual-mode MPAs, a triple-mode MPA with the frequency ratio of $f_{0,1/2}:f_{2,1}:f_{0,1} = 1.2:1.1:1$ is realized. To verify the design concept, a prototype of triple-mode MPA was fabricated and measured. Experimental results show that the proposed microstrip antenna achieves a wide bandwidth of 26.5%, a low cross-polarization of -23 dB, and high harmonic suppression.

Index Terms—Differentially-fed antenna, microstrip patch antenna, triple-resonant modes, wide bandwidth.

I. INTRODUCTION

SINCE microstrip patch antenna (MPA) has been found many applications in the wireless communication systems due to the advantages of light weight, low profile, low cost, etc. [2]. However, the inherent narrow impedance bandwidth of MPAs limit their practical applications [3]. Therefore, how to increase the bandwidth of the MPA is a primary goal of research.

In the past decades, several effective approaches [4]-[9] have been reported to enhance the bandwidth of MPA. By utilizing an optimized distributed LC circuit, an MPA with an

impedance bandwidth of 9% was achieved under a thickness of $0.043\lambda_0$ in [4]. To widen the impedance bandwidth, multilayer structures [5] and parasitic structures [6] are commonly used in the design of MPAs. However, the MPAs designed by using these methods usually suffer from high profile or bulking size. In [9], metamaterial-based patch antenna was proposed to enlarge the bandwidth of low profile MPA. This antenna achieved a bandwidth of over 26.2% within a profile height of less than $0.07\lambda_0$ by using slot coupling. However, the cross polarizations of this antenna are higher than -15 dB. Apart from the traditional methods mentioned above, novel wideband approaches were realized by reallocating different resonant modes of the printed antenna [10]-[14]. The key point of a multi-mode antenna design is how to simultaneously excite and combine three or more modes and maintain good impedance matching. In [10], by exciting and shifting $TM_{1,0}$, and $TM_{1,2}$ modes of the MPAs in proximity to each other, the MPAs obtained broad bandwidths with low profiles. In [14], three resonant modes were excited and reallocated closely to each other using slots and shorting pins to obtain a wide bandwidth of 26.2%. However, the high cross-polarization level is generated (-12.3 dB) due to the asymmetry of structure.

In this letter, a novel approach of combining multi-resonant modes to design a wideband MPA is presented. By combining the dual-mode MPA-I and II, a triple-mode wideband MPA is designed. The measured results show that the proposed antenna obtains a wide bandwidth of 26.5% (2.03-2.65 GHz) for $|S_{dd11}| < -10$ dB with a low profile of $0.047\lambda_0$. (λ_0 is the wavelength in free space at the center frequency). Meanwhile, by using the differential-feeding method, low cross-polarization level (< -23 dB) and high harmonic suppression are achieved simultaneously.

II. ANTENNA CONFIGURATION AND WORKING PRINCIPLE

A. Antenna Configuration

The configuration of the proposed differentially-fed low-profile triple-mode MPA is shown in Fig. 1. The antenna has a two-layer configuration, and it is printed on two FR4 substrates (relative dielectric permittivity $\epsilon_r = 4.4$, loss tangent $\tan\delta = 0.02$) with the same size of 170×170 mm² and thicknesses of 0.5 mm. The thickness of the air layer between the substrates is 5 mm. The triple-mode antenna is composed of three separate copper parts on Sub 1, a rectangular ground plane on Sub 2, and two rows of shorting pins that connect these two layers. The proposed antenna is simulated by using the ANSYS

This work was supported in part by the 111 Project of China, and in part by EPSRC under Grants EP/N032497/1 and EP/S005625/1. (Corresponding author: Wei Hu.)

X. Liu, W. Hu, and Y. Liu are with the National Key Laboratory of Antennas and Microwave Technology, Xidian University, Xi'an, Shaanxi 710071, China. (e-mail: weihu.xidian@ieee.org; hcmx1994@gmail.com).

S. Gao and L. Wen are with the School of Engineering and Digital Arts, University of Kent, Canterbury CT2 7NT, U.K. (e-mail: s.gao@kent.ac.uk).

Qi Luo is with the School of Physics, Engineering and Computer Science, University of Hertfordshire, Hatfield, UK, AL10 9AB e-mail: qiluo@ieee.org).

P. Fei is with the Beijing Institute of Radio Metrology and Measurement, Beijing 100854, China. (e-mail: feipeng@ieee.org).

R. Xu is with the School of Electrical and Electronic Engineering, Nanyang Technological University, Singapore 639798. (e-mail: rui.xu@ntu.edu.sg).

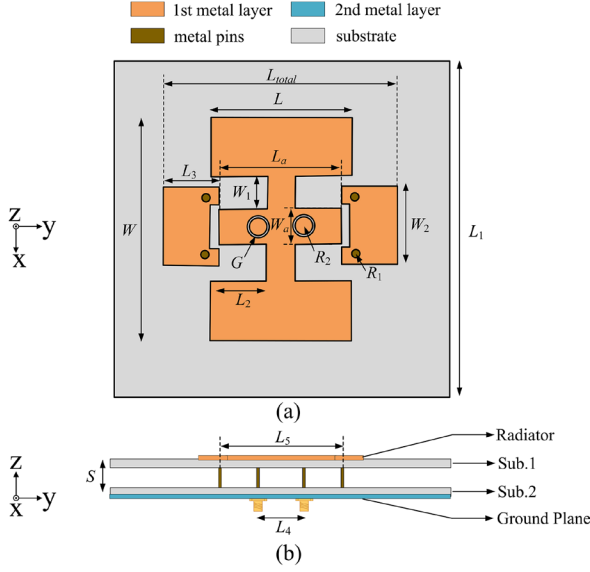


Fig. 1. Configuration of the proposed antenna. (a) Top view. (b) Side view. Dimensions are $L = 53.4$, $L_1 = 170$, $L_2 = 21.2$, $L_3 = 20$, $L_4 = 15.2$, $L_5 = 52$, $L_a = 47$ mm, $L_{total} = 86$, $W = 95$, $W_1 = 15$, $W_2 = 28$, $W_a = 15$, $R_1 = 1.2$, $R_2 = 3$, $G = 0.1$, and $S = 6$ (unit: millimeter).

HFSS.

B. MPA-I under $TM_{0,1/2}$ and $TM_{0,1}$ Modes

As described in [2] and [15], The resonant frequencies and wavenumbers of the resonant modes of an MPA can be expressed as:

$$f_{m,n} = (k_{m,n} \cdot c) / (2\pi\sqrt{\epsilon_{eq}}) \quad (1)$$

$$k_{m,n}^2 = (m\pi / W_{eq})^2 + (n\pi / L_{eq})^2 \quad (2)$$

where L_{eq} and W_{eq} are the equivalent length and equivalent width of a rectangular patch resonator, respectively. c is the speed of light in free space, $m = 0, 1, 2, \dots$, and $n = 0, 1, 2, \dots$

Without losing generality, the length L_a and the width W_a of the strip MPA are chosen to be 47 mm and 15 mm. And the input impedance of the strip MPA is shown in Fig. 2(a). Note that the input impedances in this letter are represented by Active Z_{11} . It can be seen that the strip MPA has a single resonant mode ($TM_{0,1}$ mode) at 2.4 GHz. To excite an additional resonant mode, a pair of metallic strips with shorted pins at outer edges are introduced, as shown in Fig. 2(b). The additional resonant mode appears at 2.9 GHz, while the $TM_{0,1}$ mode shifts to 1.9 GHz, and the calculated $f_{0,1/2}/f_{0,1}$ was 1.5. To incorporate these two resonant frequencies without enlarging the antenna size, the shorting pins are shifted toward the coupling gaps between the strip patch and shorted patches. It can be seen in Fig. 2(c) that the $TM_{0,1/2}$ mode is moved to 2.5 GHz while the $TM_{0,1}$ mode is shifted to 2.1 GHz. Consequently, the ratio of $f_{0,1/2}/f_{0,1}$ is reduced to 1.2.

The simulated current distributions of $TM_{0,1}$ mode and $TM_{0,1/2}$ mode are shown in Fig.3. In Fig.3(a) and (c), the current densities are concentrated on the center of the dual-mode MPA-I. In Fig.3(b) and (d), the current densities at higher

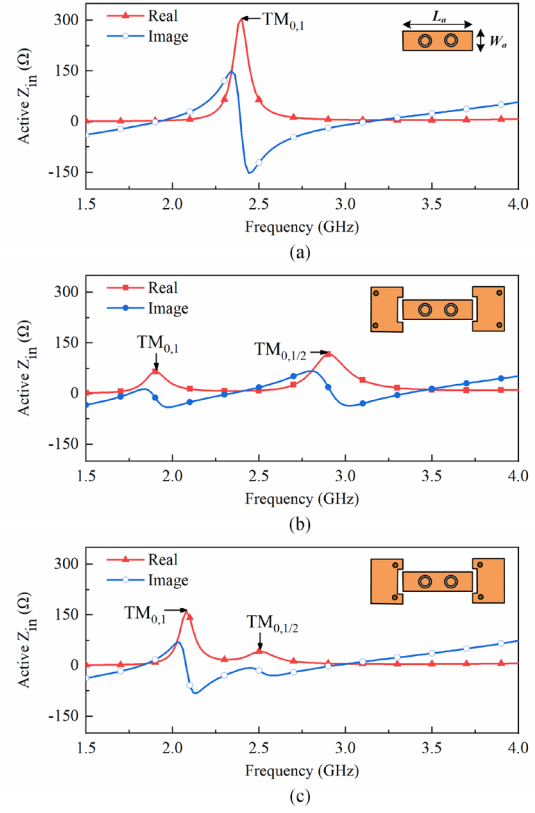


Fig. 2. Simulated input impedances of (a) Strip MPA, (b) Strip MPA with normal shorted patches, and (c) dual-mode MPA-I.

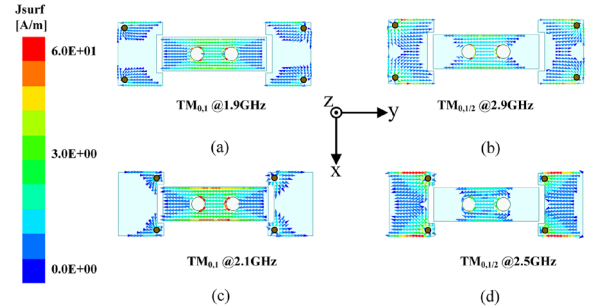


Fig. 3. Simulated current distributions of (a) $TM_{0,1}$ mode at 1.9 GHz, (b) $TM_{0,1/2}$ mode at 2.9 GHz, (c) $TM_{0,1}$ mode at 2.1 GHz, and (d) $TM_{0,1/2}$ mode at 2.5 GHz.

resonant frequency are concentrated on the sides of the dual-mode MPA-I. These results indicate that the $TM_{0,1}$ mode and $TM_{0,1/2}$ mode are successfully excited for the dual-mode MPA-I at the two resonant frequencies, respectively.

C. MPA-II under $TM_{2,1}$ and $TM_{0,1}$ Modes

Although the dual-mode MPA-I has two resonant modes, the ratio of $f_{0,1/2}/f_{0,1}$ (1.2) is still too large to form a wideband antenna. In this section, a dual-mode MPA II under $TM_{2,1}$ mode and $TM_{0,1}$ mode is designed to obtain a frequency ratio of 1.1, which is smaller than $f_{0,1/2}/f_{0,1}$ (1.2).

According to (1)-(2), the $f_{2,1}/f_{0,1}$ can be calculated by using:

$$f_{2,1} / f_{0,1} = \sqrt{(2L_{eq} / W_{eq})^2 + 1} \quad (3)$$

From (3), the ratio $f_{2,1}/f_{0,1}$ is inversely proportional to the

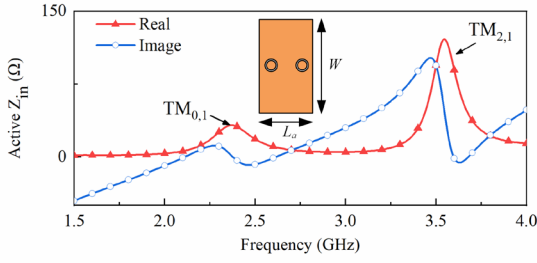


Fig. 4. Simulated input impedance of the conventional MPA.

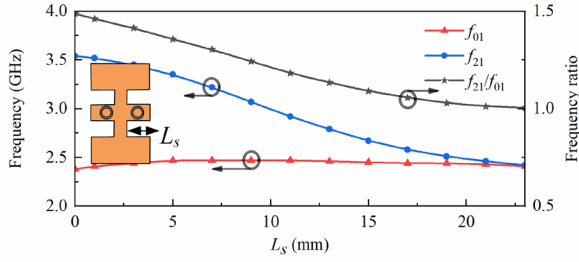


Fig. 5. Simulated resonant frequencies and corresponding ratios as a function of L_s at $TM_{0,1}$, and $TM_{2,1}$ modes.

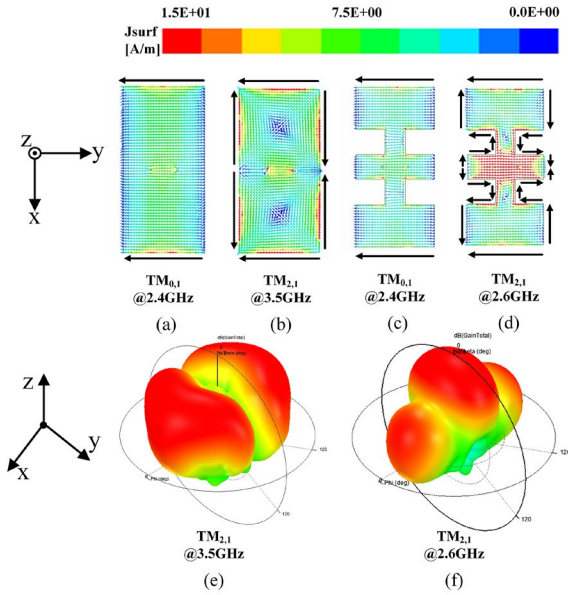


Fig. 6. Simulated current distributions of $TM_{0,1}/TM_{2,1}$ modes and radiation patterns of $TM_{2,1}$ mode.

aspect ratio. Thus, to realize a relatively small initial frequency ratio, the aspect ratio of MPA-II should be slightly large. To achieve a small initial value of $f_{2,1}/f_{0,1}$, $W = 95$ mm, and $L_a = 47$ mm are chosen to be the width and length of the patch. Therefore, the initial value of $f_{2,1}/f_{0,1}$ can be around 1.5. Fig. 4 shows the simulated input impedance of the conventional MPA using the differential feeding method. The $TM_{0,1}$ and $TM_{2,1}$ modes are excited at the same time.

To further reduce the resonant frequency ratio of $TM_{0,1}$ and $TM_{2,1}$ modes, two pairs of slots were etched on the patch. The slot length and slot width are two parameters that can be used to adjust the frequency ratio. However, the slot length L_s has much greater effects on it than the slot width W_1 . So, we set $W_1 = 15$ mm here, and adjust the frequency ratio by changing the slot

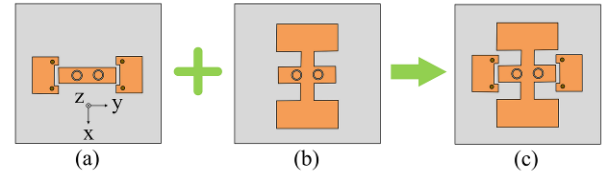


Fig. 7. Configurations of the multi-mode MPAs. (a) Dual-mode MPA-I. (b) Dual-mode MPA-II. (c) Proposed triple-mode MPA.

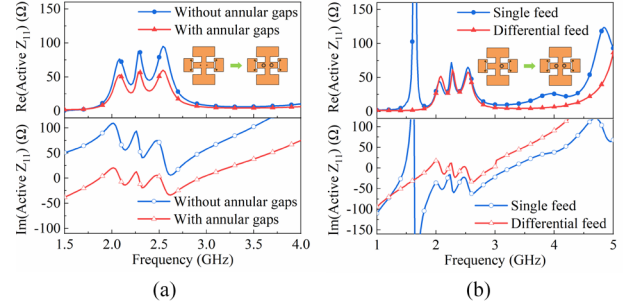


Fig. 8. Simulated input impedances of the proposed triple-mode MPA (a) with and without annular gaps, and (b) with single and differential feeds.

length L_s . As shown in Fig. 5, when the slot length (L_s) increases from 0 mm to 23 mm, the $f_{2,1}$ shifts from 3.5 GHz to 2.4 GHz, while the $f_{0,1}$ keeps nearly unchanged. When $L_s = 17.5$ mm, the desired frequency ratio of 1.1 is obtained. As shown in Fig. 6 (a) and (b), before etching the slots, the current of the $TM_{0,1}$ mode is of half-wavelength current distribution along the y-axis; the current of $TM_{2,1}$ mode shows a half-wavelength distribution along the y-axis and one-wavelength distribution along the x-axis. Due to the reverse current distribution, a split radiation pattern in the broadside direction is observed at 3.5 GHz in Fig. 6(e). After etching the slots, as shown in Fig. 6(c) and (d), the $f_{2,1}$ is shifted to 2.6 GHz because of the increased the current path along the long sides, while the $f_{0,1}$ remains unchanged. A broadside radiation pattern of $TM_{2,1}$ mode shown in Fig. 6(f) is realized owing to the concentrative in-phase current distribution in the middle of the patch. The dual-mode MPA-I and dual-mode MPA-II are finally combined, as shown in Fig. 7. It can be seen in Fig. 8(a) that a triple-mode MPA with good impedance matching is obtained with the frequency ratio of $f_{0,1}/2:f_{2,1}:f_{0,1} = 1.2:1.1:1$.

D. Capacitive Differential Feed

The annular gaps are used to compensate the additional inductance caused by the feeding probes and simultaneously adjust the input impedance of the three modes. In order to illustrate the working principle of annular gaps more clearly, the simulated input impedance of the proposed antenna with and without the annular gaps are depicted in Fig. 8(a). When the antenna is fed directly by the probes, the curve of input reactance is above the zero within the whole band due to the inductance introduced by the probes. For better impedance matching, series capacitor is formed by etching gaps between the patch and the probes. The relationship between the annular gap capacitance C_g and its gap size (G) and its inner radius (R_2) can be expressed as [16]:

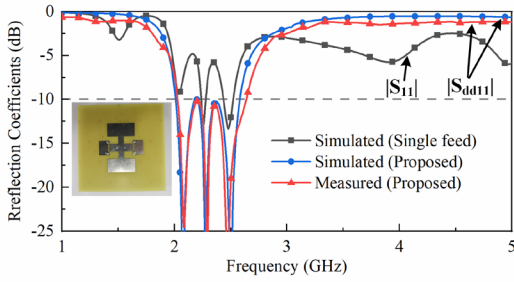


Fig. 9. Measured and simulated reflection coefficients of the proposed antenna with single and differential feed.

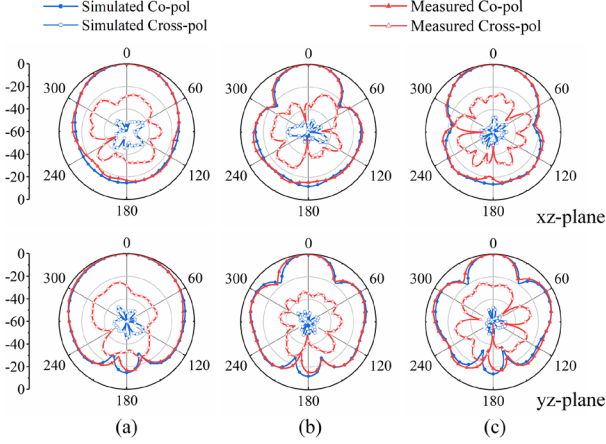


Fig. 10. Measured and simulated normalized radiation patterns for the proposed antenna at (a) 2.1 GHz, (b) 2.3 GHz, and (c) 2.5 GHz.

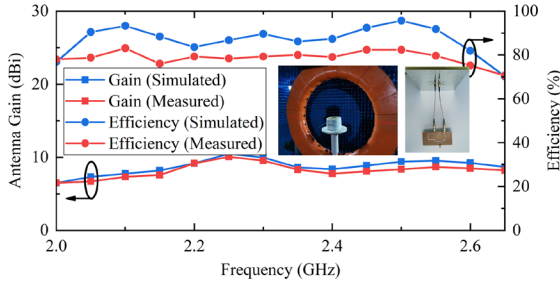


Fig. 11. Measured and simulated peak gains and efficiencies for the proposed antenna.

$$C_g \approx 4\epsilon_0\epsilon_r R_2 \cdot \ln(8R_2 / G) \quad (4)$$

By optimizing the gap size (G) and its inner radius (R_2), the input reactance can be reduced to around 0Ω , while the input resistance is slightly decreased to around 50Ω , as shown in Fig. 8(a). Besides, due to the use of the differential-feeding method, even mode of the patch can be suppressed. Simulated input impedances of the proposed triple-mode MPA with single and differential feed are shown in Fig. 8(b). It can be seen that the $TM_{2,0}$ mode at 1.6 GHz and $TM_{0,2}$ mode at 3.9 GHz are successfully suppressed by the differential-feeding scheme.

III. RESULTS AND DISCUSSION

The simulated and measured reflection coefficients are plotted in Fig. 9. Reasonable agreement between the experimental and the simulated results is obtained. The

Ref.	Height (λ_0)	BW (%)	Cross-pol (dB)	Even mode suppression
[3]	0.011	5.2	-6	No
[4]	0.043	9	NG	No
[9]	0.07	26.2	-15	No
[10]	0.039	10	-25	Yes
[14]	0.059	26.2	-12.3	No
This work	0.047	26.5	-23	Yes

* λ_0 is the wavelength at the center frequency in free space. BW is bandwidth.

multiple resonant modes are excited to achieve a good impedance matching for the bandwidth of 26.5% from 2.03 GHz to 2.65 GHz for $|S_{dd11}| < -10$ dB. Besides, high harmonic suppression is achieved with the measured $|S_{dd11}|$ higher than -2 dB from 1 GHz to 5 GHz. The differential S_{dd11} characteristics of the proposed antenna in Fig. 13 are calculated by using the formula $S_{dd11} = 1/2 (S_{11} + S_{22} - S_{12} - S_{21})$. The simulated $|S_{11}|$ of single feed antenna is obtained by using HFSS.

The radiation characteristics, including radiation patterns and antenna gains, were measured in a near-field antenna measurement system at Xidian University. A wideband out-of-phase power divider [17] was employed to realize differential feeding. Simulated and measured radiation patterns of the antenna at 2.1, 2.3, and 2.5 GHz are illustrated in Fig. 10. Radiation patterns change when different modes are excited. The measured cross-polarization (Cross-pol) is 23 dB lower than its co-polarization (Co-pol). Besides, as the frequency increases from 2.1 to 2.5 GHz, the front-to-back ratio of the radiation pattern maintains higher than 15 dB. The simulated and measured antenna peak realized gains and efficiencies are presented in Fig. 11. As shown, the proposed antenna shows an average gain of 8 dBi, and the measured efficiency of is above 70%.

Table I compares the proposed antenna with the recently reported low-profile MPAs. The present design has wider bandwidth, lower thickness and lower cross-polarization level than most of these designs.

IV. CONCLUSION

A novel approach of combining multi-resonant modes to design a wideband MPA is presented in this letter. By optimizing the position of the shorting pins, a dual-mode MPA-I with the frequency ratio of $f_{0,1/2}:f_{0,1} = 1.2$ is designed first. Then, by etching two pair of slots on conventional MPA, the radiation pattern of $TM_{2,1}$ mode is reshaped and a dual-mode MPA-II with the frequency ratio of $f_{2,1}:f_{0,1} = 1.1$ can be obtained. Finally, by combining these two dual-mode antennas and optimizing the annular gaps, a triple-mode low-profile wideband MPA frequency ratio of $f_{0,1/2}:f_{2,1}:f_{0,1} = 1.2:1.1:1$ is proposed in this letter. The measured results show that the proposed antenna achieves a wide bandwidth of about 26.5% from 2.03 to 2.65 GHz with a low profile of $0.047\lambda_0$. Besides, symmetric radiation patterns and low cross-polarization levels (< -23 dB) are realized.

REFERENCES

- [1] G. A. Deschamps, "Microstrip microwave antennas," Proc. 3rd USAF Symposium on Antennas., 1953.
- [2] G. Kumar and K. P. Ray, "Broadband microstrip antennas," Boston, Mass.: Artech House, 2003.
- [3] H. Wang, Z. Zhang, Y. Li, and Z. Feng, "A dual-resonant shorted patch antenna for wearable application in 430 MHz band," IEEE Trans. Antennas Propag., vol. 61, no. 12, pp. 6195–6200, Dec. 2013.
- [4] Y. K. Chen, S. W. Yang, and Z. P. Nie, "Bandwidth enhancement method for low profile E-shaped microstrip patch antennas," IEEE Trans. Antennas Propag., vol. 58, no. 7, pp. 2442–2447, Jul. 2010.
- [5] A. Katyal and A. Basu, "Compact and broadband stacked microstrip patch antenna for target scanning applications," IEEE Antennas Wireless Propag. Lett., vol. 16, pp. 381–384, 2017.
- [6] C. Wood, "Improved bandwidth of microstrip antennas using parasitic elements," IEE Proc. H Microw. Opt. Antennas., vol. 127, no. 4, pp. 231–234, 1980.
- [7] Y. H. Ge, K. P. Esselle, and T. S. Bird, "A compact E-shaped patch antenna with corrugated wings," IEEE Trans. Antennas Propag., vol. 54, no. 8, pp. 2411–2413, Aug. 2006.
- [8] F. Yang, X. X. Zhang, X. N. Ye, and Y. Rahmat-Samii, "Wide-band E-shaped patch antennas for wireless communications," IEEE Trans. Antennas Propag., vol. 49, no. 7, pp. 1094–1100, Jul. 2001.
- [9] B. Cheng, Z. Du, and D. Huang, "A broadband low-profile multimode microstrip antenna," IEEE Antennas Wireless Propag. Lett., vol. 18, pp. 1332–1336, 2019.
- [10] N. W. Liu, L. Zhu, W. W. CHOI, and X. Zhang, "A low-profile differential-fed patch antenna with bandwidth enhancement and sidelobe reduction under operation of TM_{10} and TM_{12} modes," IEEE Trans. Antennas Propag., vol. 66, no. 9, pp. 4854–4859, Sep. 2018.
- [11] J. Liu, Q. Xue, H. Wong, H. W. Lai, and Y. Long, "Design and analysis of a low-profile and broadband microstrip monopolar patch antenna," IEEE Trans. Antennas Propag., vol. 61, no. 1, pp. 11–18, Jan. 2013.
- [12] Z. X. Liu, L. Zhu, and N. W. Liu, "Design approach of radiation pattern reshaping for TM_{12} mode and its application in bandwidth enhancement," IEEE Trans. Antennas Propag., vol. 67, no. 7, pp. 4842–4847, Jul. 2019.
- [13] W. Hu, X. K. Liu, S. Gao, L. H. Wen, Q. Luo, P. Fei, Y. Z. Yin, and Y. Liu, "Compact wideband folded dipole antenna with multi-resonant modes," IEEE Trans. Antennas Propag., vol. 67, no. 11, pp. 6789–6799, Nov. 2019.
- [14] N. W. Liu, L. Zhu, G. Fu, and Y. Liu, "A low profile shorted-patch antenna with enhanced bandwidth and reduced H-plane cross-polarization," IEEE Trans. Antennas Propag., vol. 66, no. 10, pp. 5602–5607, Oct. 2018.
- [15] Y. Lo, D. Solomon, and W. Richards, "Theory and experiment on microstrip antennas," IEEE Trans. Antennas Propag., vol. 27, no. 2, pp. 137–145, Mar. 1979.
- [16] J. M. Kovitz and Y. Rahmat-Samii, "Using thick substrates and capacitive probe compensation to enhance the bandwidth of traditional CP patch antennas," IEEE Trans. Antennas Propag., vol. 62, no. 10, pp. 4970–4979, Oct. 2014.
- [17] Z. Y. Tang, J. H. Liu, Y. M. Cai, J. H. Wang, Y. Z. Yin, "A wideband differentially fed dual-polarized stacked patch antenna with tuned slot excitations," IEEE Trans. Antennas Propag., vol. 66, no. 4, pp. 2055–2060, Apr. 2018.